

APPLIED SCIENCES AND ENGINEERING

Noninvasive in vivo 3D bioprinting

Yuwen Chen^{1*}, Jiumeng Zhang^{1*}, Xuan Liu^{1*}, Shuai Wang¹, Jie Tao¹, Yulan Huang¹, Wenbi Wu¹, Yang Li¹, Kai Zhou¹, Xiawei Wei^{1,2†}, Shaochen Chen³, Xiang Li⁴, Xuewen Xu⁵, Ludwig Cardon⁶, Zhiyong Qian^{1†}, Maling Gou^{1†}

Three-dimensional (3D) printing technology has great potential in advancing clinical medicine. Currently, the in vivo application strategies for 3D-printed macroscale products are limited to surgical implantation or in situ 3D printing at the exposed trauma, both requiring exposure of the application site. Here, we show a digital near-infrared (NIR) photopolymerization (DNP)-based 3D printing technology that enables the noninvasive in vivo 3D bioprinting of tissue constructs. In this technology, the NIR is modulated into customized pattern by a digital micromirror device, and dynamically projected for spatially inducing the polymerization of monomer solutions. By ex vivo irradiation with the patterned NIR, the subcutaneously injected bioink can be noninvasively printed into customized tissue constructs in situ. Without surgery implantation, a personalized ear-like tissue constructs with chondrification and a muscle tissue repairable cell-laden conformal scaffold were obtained in vivo. This work provides a proof of concept of noninvasive in vivo 3D bioprinting.

INTRODUCTION

Three-dimensional (3D) printing technology, an advanced additive manufacturing technology, has advantages in fabricating personalized or complex structures with wide medical applications. Bioprinting, i.e., use of bioink containing cells to 3D print living obstacles such as tissue or organ, has great potential in advancing medicine, especially in regeneration medicine (1–5). Currently, commonly used 3D bioprinting systems include inkjet printing (6, 7), extrusion printing (8), light-assisted printing (3, 9–12), and laser direct writing (13). Currently, the in vivo application strategies for 3D-printed macroscale products are limited to surgical implantation or in situ 3D printing at the exposed trauma, both requiring exposure of the application site. However, a major trend of clinical treatments is minimally invasive or noninvasive approaches (14, 15). For internal injuries under the skin, surgery exposing trauma would damage the surrounding tissues, causing a secondary injury. Meanwhile, for plastic surgery, noninvasive methods are very desired. These important clinical requirements cannot be well met by the existing 3D printing technologies, motivating us to develop noninvasive 3D printing technologies that can noninvasively fabricate the tissue-covered bioink into customized products, including living tissue constructs in situ.

Digital light processing (DLP)-based 3D bioprinting technology, a light-assisted bioprinting method, has attracted much attention in recent decades for its high cell viability of postprinting and superior printing speed and resolution (3, 9, 10). Currently, it has been rationally used for multiple-tissue reconstruction or repair, including spinal cord (3), peripheral nerve (16), and blood vessel injury (17).

Conventionally, ultraviolet (UV) or blue light is exploited to assist bioprinting via photopolymerization. However, it is difficult to use UV or blue light as a tool for noninvasive manufacturing because of the poor tissue-penetration capacity. Near-infrared (NIR) light can penetrate into deep tissue and has been used for controlled drug release (18), photodynamic therapy (19), photothermal therapy (20), in vivo imaging (21), 3D image visualization (22), and optogenetics in vivo (23). Moreover, similar to UV or blue light, NIR light has potential to initiate photopolymerization. The NIR-induced photopolymerization provides a transformative method for noninvasive fabrication in vivo. The precise control of the NIR-induced efficient photopolymerization enables the noninvasive fabrication of the tissue-covered bioink into structured products, with potential application in clinic or medical research. In this study, on the basis of the design of a digital NIR photopolymerization (DNP) process, we develop a noninvasive in vivo 3D bioprinting system. In this system, by inputting a computer-aided design (CAD) model, the digital NIR is dynamically generated by the connected digital micromirror device (DMD) chip and timely projected to noninvasively induce the spatial polymerization of the local injected bioink layer by layer. Without surgery implantation, customized living tissue constructs were successfully generated in the body. This work would open a new avenue for 3D printing research and advance the noninvasive medicine field.

RESULTS

Taking the advantage of good tissue penetration of NIR light, we designed a noninvasive 3D printing technology based on DNP process, as schematically shown in Fig. 1. In this technology, the NIR light beam is timely modulated by a DMD, subsequently projected into customized pattern by lens. The patterned NIR penetrates through the skin to induce the spatial polymerization of subcutaneously injected monomer solution containing cells. By a nanoinitiator, the commonly used biocompatible hydrogel monomers such as gelatin methacryloyl (GelMA) can be efficiently initiated for polymerization under NIR irradiation. After the images were fed to the computer in sequence, the monomer solution containing cells as a bioink could be noninvasively printed into customized tissue constructs in vivo.

¹State Key Laboratory of Biotherapy and Cancer Center, West China Hospital, Sichuan University, Chengdu 610041, P. R. China. ²Laboratory of Aging Research and Cancer Drug Target, State Key Laboratory of Biotherapy, National Clinical Research Center for Geriatrics, West China Hospital, Sichuan University, Chengdu 610041, P. R. China. ³Department of Nanoengineering, University of California San Diego, San Diego, CA, USA. ⁴Department of Urology, Institute of Urology, West China Hospital, Sichuan University, Chengdu 610041, P. R. China. ⁵Department of Aesthetic Plastic and Burn Surgery, West China Hospital, Sichuan University, Chengdu 610041, P. R. China. ⁶Centre for Polymer and Material Technologies, Department of Materials, Textiles and Chemical Engineering, Ghent University, Ghent 9052, Belgium.

*These authors contributed equally to this work.

†Corresponding author. Email: goumaling@scu.edu.cn (M.G.); anderson-qian@163.com (Z.Q.); xiaweiwei@scu.edu.cn (X.W.)

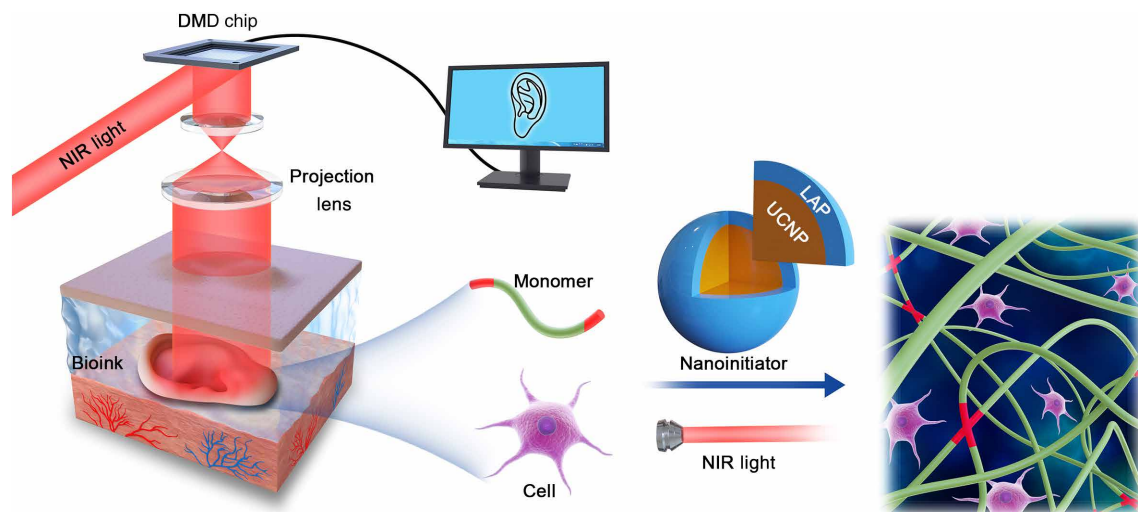


Fig. 1. Schematic diagram of DNP-based noninvasive 3D bioprinting. The data of a customized CAD model were sent into the DMD chip through a control computer. The 980-nm NIR light with an optical pattern was casted across optical lens, and tissue onto the bioink, which was injected into the body to noninvasively fabricate a living tissue in vivo. The bioink contains UCNP@LAP nanoinitiators that can convert the NIR light to 365-nm light and then initiate the optical pattern–controlled polymerization of monomers.

Nanoinitiators for NIR-induced polymerization

In the DNP process, a nanoinitiator, i.e., an up-conversion nanoparticle (UCNP) (24) coated with UV/blue-light photoinitiator (PI) lithium phenyl-2,4,6-trimethylbenzoylphosphinate (LAP) (25), was designed and called UCNP@LAP. The design was motivated by the fact that the nanoinitiator providing up-conversion UV photons emitted from UCNPs under NIR irradiation was absorbed by LAP to initiate photosensitive monomer polymerization and to avoid the UV detrimental effect on cells. After optimization of the elemental compositions including Yb and Tm, the UCNPs with good UV-region up-conversion efficiency were prepared (figs. S1 and S2). The obtained aqueous UCNPs were highly crystalline and had hexagonal morphology, with a mean particle size of ~ 60 nm (Fig. 2A and fig. S3). By coating UCNPs (positive) with LAP (negative) through electrostatic interactions, UCNP@LAP nanoinitiators were readily prepared. After coating with LAP, the ζ potentials of UCNPs decreased from 53.1 ± 9.8 mV to -3.9 ± 3.56 mV (fig. S4A). Compared to the UCNPs, the UCNP@LAP nanoparticles showed an obvious shell structure (Fig. 2A). In addition, the successful coating of LAP was verified by Fourier transform infrared (FTIR) and energy-dispersive x-ray analysis (figs. S4B and S5). The corresponding element mappings confirmed the chemical compositions of Y and P in the nanoinitiator (Fig. 2B). The thermogravimetric analysis (TGA) indicated that the content of LAP in the purified UCNP@LAP nanoinitiator was 12% (Fig. 2C). Figure 2D shows the absorption spectrum of LAP (blue line) and up-conversion luminescence emission spectra of UCNPs (purple line) and UCNP@LAP nanoinitiators (black line) in an aqueous solution upon 980-nm excitation. The UCNPs showed up-conversion emission peaks at 345 and 361 nm under the excitation of 980-nm light. The specific emission bands of the UCNPs had good overlap with the absorption band of LAP. Compared to the UCNPs, the UV-region emission (320 to 380 nm) of the UCNP@LAP nanoinitiators disappeared, indicating that the UV photon delivered by UCNPs could be efficiently absorbed by the LAP of the outer shell (Fig. 2D). As a result, the absorption band

of the acylphosphinate chromophore of LAP at 371 nm decreased with the increase in NIR light time intervals, exhibiting excellent photobleaching behavior of the nanoinitiators (fig. S6). After the exposure of NIR light for about 15 s, the precursor solution containing 15 weight % (wt %) GelMA and 1 wt % UCNP@LAP nanoinitiators could be polymerized into hydrogels (fig. S7). A test of photocuring ratio was conducted to evaluate the efficiency of UCNP@LAP nanoinitiators under various exposure times and powers of the NIR light (26). As shown in Fig. 2 (E and F), the photocuring ratios were found to increase with the increase in exposure time and the power of NIR light. Polyacrylic acid (PAA) was used for surface modification of UCNP to avoid LAP coating. Degrees of photocuring ratio of GelMA versus time under NIR light for UCNP@LAP, UCNP@LAP and PAA, and UCNP@PAA and LAP were tested. As shown in fig. S8, the efficiency of the UCNP@LAP nanoinitiator was higher than that of the UCNP and LAP mixture system (fig. S8). These results indicate that the designed UCNP@LAP nanoparticles can work as an efficient initiator to initiate the NIR-induced polymerization of commonly used hydrogel monomers.

Potential of the DNP process in bioprinting

First, the potential of the DNP process in bioprinting was evaluated in vitro. Because of the excellent capacity of supporting cells for survival or proliferation, biocompatible hydrogels are commonly used as the matrix materials for bioprinting. Here, we found that the DNP process could fast print the GelMA-derived hydrogel obstacles by a layer-by-layer manner, and the time of printing a 200- μ m-thick layer is about 15 s. Then, the capacity of the DNP process in 3D printing of complex hydrogel constructs was evaluated. As shown in Fig. 3A, three-ring microconstructs with decreasing widths from 200 to 100 μ m could be precisely fabricated using this DNP process. Moreover, complex 3D structures, such as double-layered microstructures with Danboard-like and flower-like shapes, three-layered microstructure with round cake-like shape, and a type of truss structure, could also be readily fabricated ex vivo (Fig. 3A). This indicates

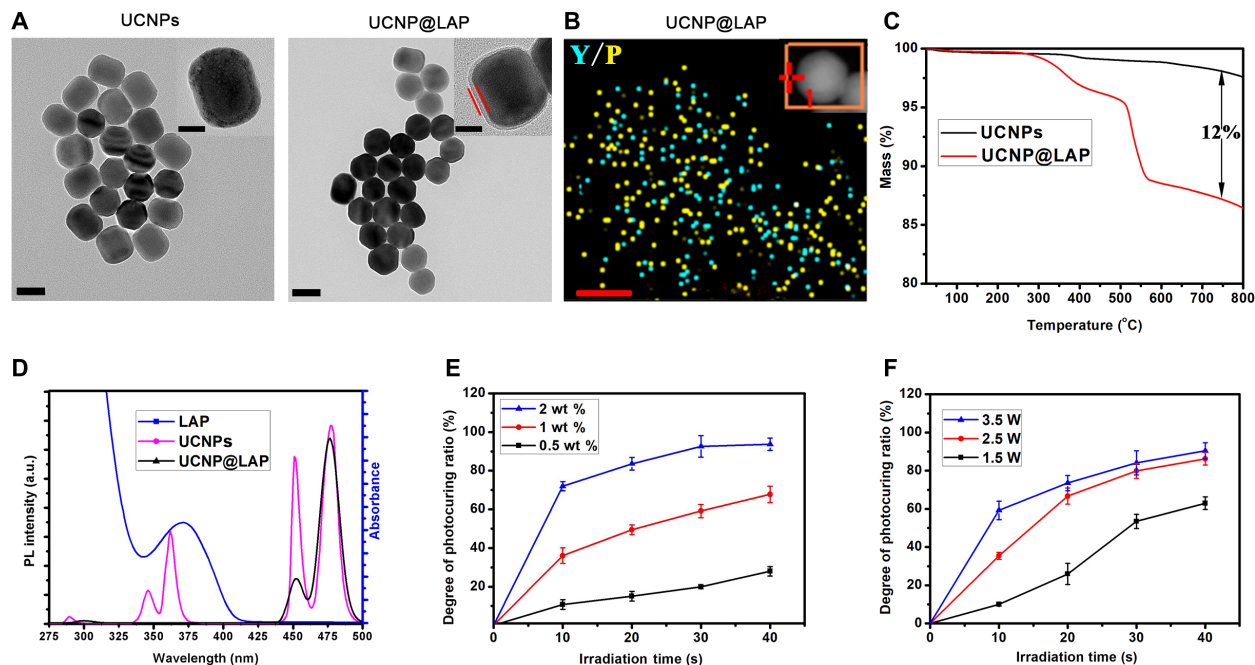


Fig. 2. Characterization of UCNP@LAP nanoinitiators. (A) Transmission electron microscopy images of aqueous UCNPs and UCNP@LAP nanoinitiators. UCNP@LAP nanoinitiators show an obvious shell structure. Scale bars, 20 (top) and 50 nm (bottom). (B) Elemental mapping of a single UCNP@LAP nanoinitiator, indicating the distribution of Y and P elements. Scale bar, 20 nm. (C) Thermogravimetric analysis (TGA) curves of UCNPs (black line) and UCNP@LAP nanoinitiators (red line) of the analyses performed under N_2 atmosphere. (D) Absorption spectrum of LAP (blue line) and up-conversion luminescence emission spectra of UCNPs (purple line) and UCNP@LAP nanoinitiators (black line) in aqueous solution upon 980-nm excitation. a.u., arbitrary units. (E) Degree of photocuring ratio of GelMA (15 wt %) versus time under 2-W NIR light for various concentrations of UCNP@LAP nanoinitiators: 0.5 (black), 1 (red), and 2 wt % (blue). (F) Degree of photocuring ratio versus time using UCNP@LAP (1 wt %) as the PIs for various powers of NIR light: 1.5 (black), 2.5 (red), and 3.5 W (blue). PL, photoluminescence.

that the DNP process has potential application in precise printing of customized 3D structures.

Then, the feasibility of the DNP process in noninvasive in vivo 3D printing was studied using an ex vivo model. As shown in Fig. 3B, a piece of mice skin or 0.5-mm-thick pig muscle tissue was covered on the bioink to mimic the phenomena of the noninvasive in vivo 3D bioprinting. As shown in Fig. 3C, the NIR light with a circle pattern could efficiently penetrate through the skin or muscle, to excite a patterned emission from the UCNP@LAP nanoinitiators in the bioink, and subsequently induce polymerization. Under the coverage of skin or muscle, circle microconstructs could be successfully printed. Compared to the control group, the coverage of skin or muscle tissue did not substantially affect the printing quality in this experiment (Fig. 3C). ImageJ software was used to calculate the areas of the printed constructs. The extent of defect of the construct that printed from the bioink covered by muscle is 12.1%. These results indicate the potential application of DNP process in noninvasive in vivo 3D bioprinting.

Moreover, the promise of the DNP process in noninvasive in vivo 3D printing was studied in vivo. After 50 μ l of a precursor solution was subcutaneously injected into the BALB/c mice, the data of a CAD model were sent into the DMD chip through the computer, to create a customized NIR pattern to polymerize the monomer solution in vivo. Considering the difference between in vitro and in vivo concentration of oxygen that can scavenge free radicals to inhibit polymerization (27, 28), we studied the effect of oxygen level on NIR-induced polymerization. After purging with nitrogen to degas oxygen, photocuring occurred within 20 s at a low concentration (0.5 wt %)

of UCNP@LAP (fig. S9). This indicates that the inhibition of oxygen could improve the NIR-induced free-radical polymerization, as could also be supported by previous studies (27, 28). Compared with the in vitro condition, the in vivo condition that often has lower oxygen concentration might facilitate the DNP-based process for bioprinting. The hematoxylin and eosin (H&E) staining of tissues surrounded to the noninvasively printed hydrogel constructs was performed to determine the potential side effect of this DNP process. The results show that, 1 or 7 days after printing, the surrounding tissues have complete tissue structures without significant inflammation and abnormal defects (Fig. 4A). This indicates that the DNP-based noninvasive bioprinting process did not cause obvious side effect in situ. To evaluate the flexibility of DNP process in noninvasive bioprinting in vivo, we designed and printed different structures. As shown in Fig. 4B, three types of structures, including triangle, cross, and two-layer cake-like hydrogel constructs, were successfully noninvasively printed by the DNP process in vivo. This indicates that the DNP process has potential for noninvasive in vivo 3D bioprinting.

Noninvasive in vivo 3D bioprinting for tissue reconstruction or repair

Auricle defect caused by congenital malformation (microtia) or trauma is one of the common diseases that can critically affect the patients' psychological and physiological well-being. The regional prevalence rate of microtia varies from 0.83 to 17.4 per 10,000 births worldwide, with higher prevalence rates in Asians (29). Auricle defect often needs the implantation of artificial auricle in vivo (29, 30). While the implantation process would cause iatrogenic injury, a noninvasive

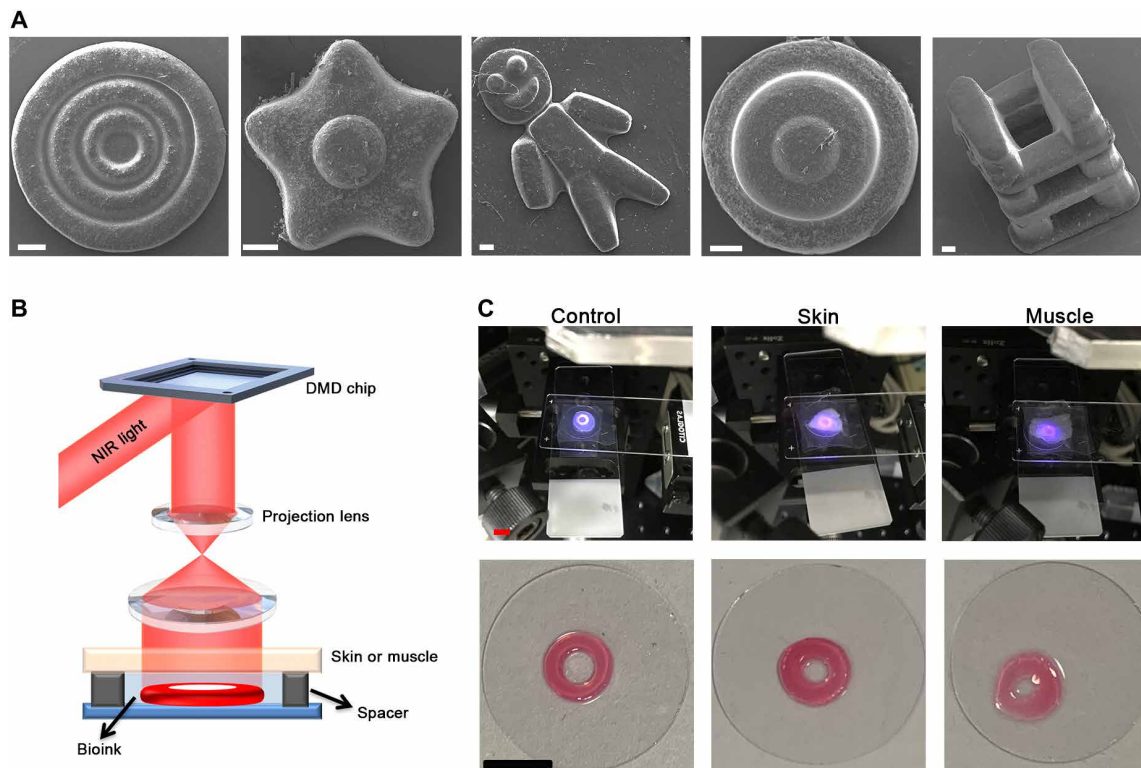


Fig. 3. 3D bioprinting acellular constructs using DNP-based process in vitro. (A) Scanning electron microscopy (SEM) images of fabricated constructs including three-ring microconstructs with decreasing widths, flower-like, Danboard-like, round cake-like, and a type of truss constructs. Scale bars, 200 μm . (B) Schematic diagram of printing setup used to estimate the tissue-penetration capacity. The bioink was deposited under the skin or muscle. (C) The images of ring constructs printed from bioink (control) or bioink covered over by skin or 0.5-mm-thick muscle by DNP process. Scale bars, 0.5 cm. Photo credit: Yuwen Chen, State Key Laboratory of Biotherapy and Cancer Center.

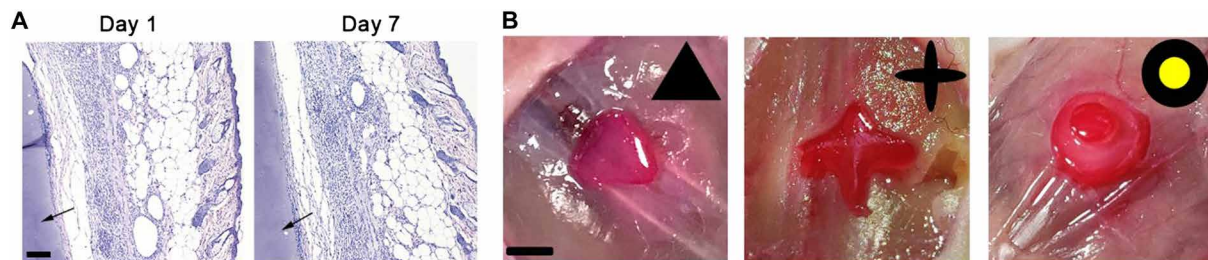


Fig. 4. 3D bioprinting acellular constructs by DNP-based process in vivo. (A) H&E of the surrounding tissue of construct after DNP printing in vivo for 1 and 7 days. The arrow represents the printed construct. Scale bar, 100 μm . (B) CAD models and vitamin B12-stained triangle, cross, and two-layer cake-like constructs fabricated by noninvasive DNP-based process in vivo. Scale bar, 0.5 cm. Photo credit: Jiumeng Zhang, State Key Laboratory of Biotherapy and Cancer Center.

process is very desired for both patients and doctors. Here, we performed an attempt to use the DNP process to noninvasively prepare a customized ear-like living construct in vivo. As shown in Fig. 5C, a personalized ear shape (Fig. 5C) was acquired according to the mirror image (Fig. 5B) of the other healthy ear (Fig. 5A). Under the coverage of skin, the ear-shaped construct containing chondrocytes could be printed in vitro (Fig. 5D). The cells had good viability after printing and culture for 7 days in vitro (cell viability, >80) (Fig. 5E). Moreover, DNP-based noninvasive in vivo 3D bioprinting was performed. The bioink containing chondrocytes were subcutaneously injected into mice, followed by illumination with the digital NIR encoding of the personal ear shape. Twenty seconds later, the ear-shaped construct was noninvasively printed in vivo (Fig. 5F). After

1 month, the ear shape of the construct was maintained (Fig. 5G). The histological analysis showed the chondrocyte ovoid lacunae with collagen type II secretion in the extracellular matrix (Fig. 5, H and I). Together, with the growth of chondrocytes, the ear-like tissue formed in situ. The customized ear-like living construct has promising application in future tissue regeneration and auricle reconstruction. These results indicate that the DNP-based noninvasive in vivo 3D bioprinting technology has potential in preparing complex tissues in situ for organ reconstruction, with minimal iatrogenic injuries.

Closed injuries with tissue defects can be caused by multiple reasons such as crushed by blunt force (31). Local delivery of stem cells such as adipose-derived stem cells (ASCs) can promote the tissue

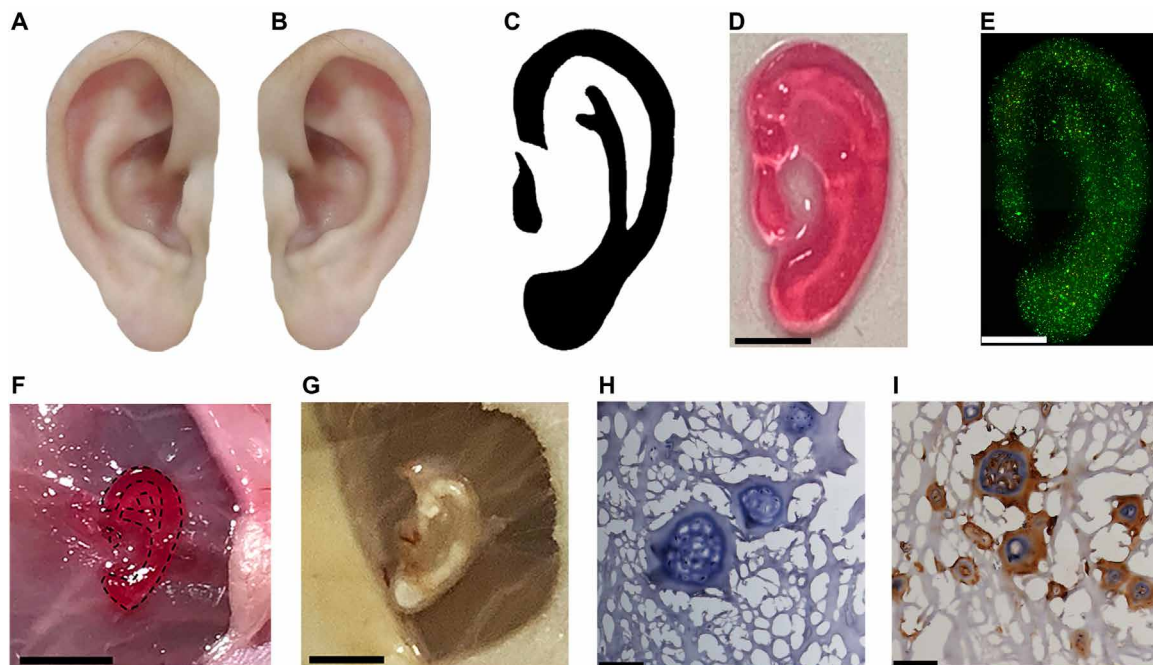


Fig. 5. Noninvasive 3D bioprinting ear-like tissue by the DNP-based process. (A) Representative image of the normal ear. (B) Mirror image of (A). (C) Optimized ear-outline image of (B). (D) Image of printed ear-like construct from the bioink covered over by skin by DNP process. Scale bar, 2 mm. (E) The Live/Dead staining for ear constructs encapsulated with chondrocytes bioprinted from bioink covered by skin after culture for 7 days. Scale bar, 2 mm. (F) Noninvasive 3D bioprinting of ear-shaped construct in vivo by DNP-based process. The ear-shaped construct was printed subcutaneously in BALB/c nude mice. Scale bar, 5 mm. (G) Representative image of bioprinted ear-shaped construct at 1 month. Scale bar, 5 mm. (H) H&E and (I) collagen type II immunostaining of retrieved ear-shaped construct at 1 month. Scale bars, 50 μm . Photo credit: Yuwen Chen, State Key Laboratory of Biotherapy and Cancer Center.

regeneration (32, 33). A conformal scaffold containing ASCs has potential application in repairing the tissue defect. Noninvasive installation of the conformal cell-laden scaffolds into the defect could avoid the implantation process–caused iatrogenic injury. Here, a conformal ASC-laden scaffold was noninvasively printed in situ for promoting the healing of the muscle defect in vivo. First, an excisional muscle wound healing model was built in BALB/c mice (Fig. 6A). Then, to match the wound shape, an ASC-laden scaffold with 8-mm triangle shape was noninvasively printed by the DNP process in situ. After 10 days, the treatment group showed significant improvement in wound closure compared to the control group (Fig. 6, B and C). The histological analysis, as shown in Fig. 6D, shows that the formation of muscle tissue of the treatment group was significantly better than that of the control group. This indicates that the ASC-laden conformal scaffold could accelerate the wound healing. Meanwhile, H&E staining showed that this treatment did not cause significant systemic toxicity in vivo (fig. S10). Therefore, the noninvasive in vivo 3D bioprinting of conformal cell-laden scaffold in situ have potential application in tissue repair for closed-injury treatment.

DISCUSSION

A disruptive technology is a new technology that has major promoting effect on technologies that existed before. Disruptive technologies can create products and services becoming significantly better, cheaper, and more convenient. Meanwhile, they also offer a revolutionary change in the conduct of operations or processes. 3D printing is recognized as a disruptive technology, emerging in recent years that could revolutionize the manufacturing technologies in multiple fields,

including manufacturing engineering, electronics fabrication, and materials and artificial tissues. Currently, lack of advanced 3D printing technologies is one of the major challenges for the development of 3D-printed products. The DLP-based 3D printing technology provides an advanced bioprinting tool for regeneration medicine and drug development. Recently, some progresses have been made to improve the speed, resolution, or scales (34, 35). Meanwhile, the progresses in bioprinting technology have led to the advance of medicines, such as the 3D-printed lung-like organ constructs (36), heart-like organ constructs (5), and scaffolds for spinal repair (3). However, different medical applications always mean different requirements to the 3D printing technology. One 3D printing system is often difficult to satisfy the requirements of different medical applications. Therefore, it is very important to customize 3D printing systems for the specific medical applications. In this work, to meet the requirement of minimally invasive or noninvasive medicine, we demonstrated a DNP-based noninvasive in vivo 3D bioprinting. To the best of our knowledge, this work might be the first report for the DNP process and the noninvasive in vivo 3D bioprinting, which could inspire the development of novel 3D bioprinting technologies.

For photopolymerization, a commonly used light source is UV light. However, the UV light always injures cells, and its tissue-penetration ability is limited, leading to the limitation in bioprinting. Because of the good biocompatibility, blue light has attracted much attention in bioprinting in recent years. For the DNP process, it is essential to use NIR light. Because of the low-energy characteristic of NIR photon and the inadequate photon absorption of initiators, challenges remain to efficiently induce polymerization by NIR light. Currently, some organic molecules such as bacteriochlorophyll a (37)

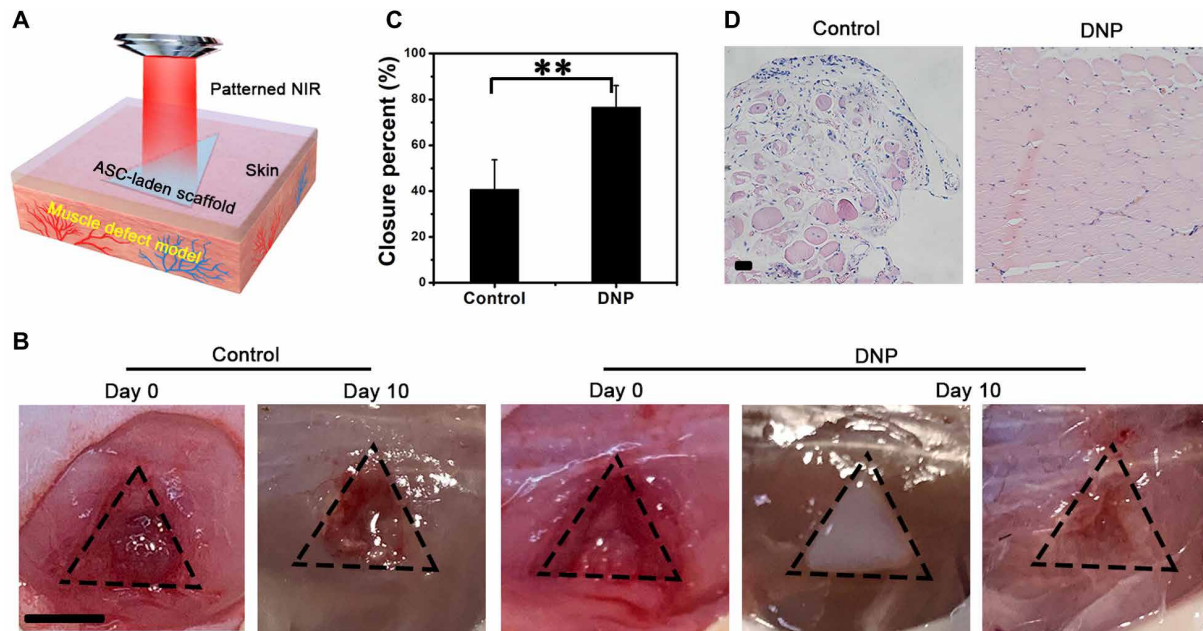


Fig. 6. Noninvasive 3D bioprinting conformal ASC-laden scaffold for muscle defect repair by the DNP-based process. (A) Schematic illustration of the conformal ASC-laden scaffold for muscle defect repair. (B) Representative images exhibit acceleration of the wound healing of the DNP group compared with control. Scale bar, 5 mm. (C) Percent closure of muscle wounds evaluated at day 10. $**P < 0.01$, $n = 5$. (D) H&E histological analysis of muscle wound healing at day 10 after treatments. Scale bar, 50 μm. Photo credit: Yuwen Chen, State Key Laboratory of Biotherapy and Cancer Center.

and dye borate (38) have been found as initiators for NIR-induced polymerization. However, it is difficult to use these hydrophobic initiators directly in the preparation of hydrophilic hydrogel system. With the development of up-conversion materials such as UCNPs, NIR can be converted into UV to induce photopolymerization, providing an alternative method for developing novel NIR-induced polymerizations. Previously, some attempts have been made to use NIR light to induce polymerization of a monomer solution containing UCNPs and UV-visible (UV-Vis) light-sensitive PIs, where the efficiency still needs improvement (13, 39). In this study, we designed a LAP-coated UCNPs nanoparticle as a nanoinitiator for NIR-induced polymerization. The LAP can efficiently absorb UV photons emitted from UCNPs under NIR irradiation. The detrimental effect of its UV emissions on cells can be avoided owing to UCNPs@LAP that mainly emitted visible light. Meanwhile, the efficiency of the UCNPs nanoinitiators was higher than that of the UCNPs and LAP mixture system. This might be due to that the LAP coating on UCNPs could minimize the water-quenching effect of its up-conversion luminescence, resulting from attenuating the surface contact between UCNPs and water (40). In this work, the UCNPs@LAP nanoinitiators solidly support the noninvasive in vivo 3D bioprinting technology by improving the NIR-induced polymerization efficiency and the printing speed. Moreover, the design cue of LAP@UCNPs nanoinitiator might inspire the development of more efficient initiators for NIR-induced polymerization.

Tissue defects or injuries are common diseases that often cause death or disability. Stem cells have great promise for tissue reconstruction or repair to treat tissue defects or injuries (3, 30). As a minimally invasive or noninvasive method, injection is well accepted to introduce therapeutics into the body for disease treatment. However, directly injected cells often have low survival and unsatisfied tissue distribution in vivo. To address this issue, we coated cells by

biomaterials to improve the survival and tissue distribution in the focus. Meanwhile, the injected cells or cell-loaded microparticles are very difficult to form a complex tissue or organ in vivo for the treatment of complex tissue defects such as the auricle defect. Conventionally, the tissue constructs are first prepared ex vivo and then implanted in situ. In this process, it is very difficult to avoid the surgery that often causes iatrogenic injury. Recently, some attempts have also been made to obtain simple and small-sized structures by the self-assembly of the injected microparticles (41, 42). Also, some shape memory materials were designed for the minimally invasive or noninvasive medicine (43). Despite these progresses, it is still challenging to create a complex tissue construct in vivo via a minimally invasive or noninvasive method. Moreover, customized tissue constructs are often needed for the tissue reconstruction or repair. Here, taking the advantages of 3D printing in the fabrication of personalized or complex structures, we demonstrate a novel DNP-based 3D printing technology for the noninvasive fabrication of customized tissue constructs from the injected bioink containing cells. Using this DNP technology, the customized ear-shaped tissue construct was noninvasively printed in situ and gradually be chondrified with time, showing potential application in treating auricle defect or microtia. Meanwhile, the noninvasively printed conformal ASC-laden scaffold can promote the healing of the muscle defects, showing potential clinical application. Therefore, the demonstrated noninvasive in vivo 3D bioprinting technology could provide a novel tool to advance the minimally invasive or noninvasive medicine, showing potential clinical applications.

In summary, this work solidly contributes to proposing the new concept of noninvasive in vivo 3D bioprinting, i.e., noninvasive 3D printing of the bioink in body into customized biomedical products, including living tissues in situ. The bioink is locally introduced in body by minimally invasive or noninvasive methods, such as

injection and perfusion. The spatial consolidation of the bioink is induced by noninvasive tools, such as the digital NIR and magnetic field. Future researches in the noninvasive in vivo 3D bioprinting field would significantly advance the related technologies and clinical applications.

CONCLUSION

This work demonstrates a DNP-based bioprinting system, where the complex constructs can be fabricated layer by layer using UCNP@LAP nanoparticle-initiated NIR polymerization. By this system, customized living constructs can be noninvasively printed in vivo from the subcutaneously injected bioink, for organ reconstruction or tissue repair, showing potential clinical application. This work provides the proof of concept for the noninvasive in vivo 3D bioprinting that would open a new avenue for medical 3D printing and advance the minimally invasive or noninvasive medicine.

MATERIALS AND METHODS

Anhydrous YCl_3 (99.9%), anhydrous YbCl_3 (99.9%), anhydrous TmCl_3 (99.9%), NaOH (>98%), oleic acid (90%), PAA ($M_n = 5100$), and type A gelatin and methacrylic anhydride (MAA; 94%) were purchased from Sigma-Aldrich. Anhydrous YCl_3 (99.99%), 1-octadecene (90%), NH_4F (>98%), and dimethyl phenylphosphonite (98%) were purchased from Alfa Aesar. 2,4,6-Trimethylbenzoyl chloride (98%) was purchased from Adamas. All the chemicals were of analytical grade and were used as received without further purification. The newborn rat, BALB/c nude mice, and BALB/c mice were purchased from Beijing Huafukang Bioscience Co. Inc. and kept in an animal house. All the animal studies were carried out in compliance with the guidelines on animal care and at State Key Laboratory of Biotherapy, Sichuan University, China.

Synthesis of aqueous UCNPs

Aqueous UCNPs were synthesized using a modified method (24). In a typical synthesis of UCNP cores: $\text{NaYF}_4\text{:Yb,Tm}$ (30/0.3 mole percent), YCl_3 (108.3 mg, 0.556 mmol), YbCl_3 (67.0 mg, 0.24 mmol), and TmCl_3 (1.1 mg, 0.004 mmol) were added to a 100-ml flask containing 6 ml of oleic acid and 14 ml of 1-octadecene. Then, the solution was slowly heated to 140°C under vacuum for 1 hour until a homogeneous transparent light yellow solution was obtained. Then, 10 ml of methanol solution of NH_4F (118.4 mg, 3.2 mmol) and NaOH (80 mg, 2 mmol) were added, and the resulting cloudy mixture was stirred for 30 min at 50°C. The methanol was distilled off. The solution was heated to 300°C quickly under the N_2 flow and kept for 1.5 hours. The mixture was precipitated by the addition of 20 ml of ethanol, and the precipitate was collected by centrifugation at 6500 rpm for 5 min. After washing four times, the final product $\text{NaYF}_4\text{:Yb,Tm}$ was redispersed in 4 ml of cyclohexane.

Four milliliters of preprepared $\text{NaYF}_4\text{:Yb,Tm}$ (dispersed in cyclohexane) was reacted with YCl_3 in a 100-ml flask containing oleic acid and 1-octadecene. The next procedures were performed as same as synthesis of UCNP cores. The product was collected by centrifugation and then redispersed in 0.1 M HCl solution. The mixture was then sonicated at 45°C for 1 hour to remove the oleate ligands. The product was redispersed in acetone, and the particles were recuperated by centrifugation. Last, the nanoparticles were dispersed in water at a concentration of 50 mg/ml.

Synthesis of the PI LAP

2,4,6-Trimethylbenzoyl chloride was reacted with dimethyl phenylphosphonite via a Michaelis-Arbuzov reaction (25). The structure of LAP was confirmed by ^1H nuclear magnetic resonance (NMR). ^1H NMR (400 MHz, D_2O) δ 7.79 to 7.72 (m, 2H), 7.64 to 7.58 (m, 1H), 7.54 to 7.49 (m, 2H), 6.93 (s, 2H), 2.28 (s, 3H), and 2.07 (s, 6H).

Preparation of UCNP@LAP nanoinitiators

The nanoinitiators were prepared by coating UCNP (positive) and LAP (negative) through electrostatic interactions. A solution of LAP (50 mg) dissolved in ionized water was added dropwise to an aqueous solution containing 50 mg of UCNPs with ultrasonication, and the resulting mixture was sonicated for several hours. The purified UCNP@LAP nanoinitiators were obtained followed by centrifugation.

Synthesis of GelMA

GelMA was synthesized, as previously reported (44). Gelatin (10 g) was dissolved in an aqueous solution of 100 ml of Na_2CO_3 (0.63 g) and NaHCO_3 (1.47 g). MAA (1 ml) was added dropwise to the gelatin solution under stirring at 50°C. After 3 hours, the pH was adjusted to 7 by adding 6 M HCl to stop the reaction. GelMA was obtained after filtration, dialysis, and lyophilization.

Characterization

^1H NMR spectra were recorded using a Bruker 400-MHz spectrometer. Transmission electron microscopy images were acquired on a Tecnai G2 F20 S-TWIN electron microscope operating at 200 kV. Scanning electron microscopy (SEM) image was performed on a JSM-7500F electron microscope operating at 30 kV. FTIR spectra were recorded on a Nicolet 6700 spectrophotometer. x-ray diffraction measurements were carried out at room temperature equipped an Empyrean diffractometer using $\text{Cu K}\alpha$ radiation. UV-Vis spectra were recorded on a UV-3101PC Shimadzu spectroscope. Up-conversion luminescence emission spectra were recorded on a Fluorescence Spectrometer F-7000 instrument equipped with an external 980-nm semiconductor laser (Changchun Laser Optoelectronics Technology Co. Ltd.).

Photocuring ratio test

To evaluate how the curing ratio is affected by concentration, irradiation time, and NIR light power, a photocuring ratio test was conducted (26). During irradiation time points of 10, 20, 30, and 40 s, an aqueous ink containing GelMA (15 wt %) and different concentrations of UCNP@LAP nanoinitiators or different NIR light (980 nm) power were tested. The aqueous ink was dried in vacuo and weighed (W_0). The NIR-cured aqueous ink was washed with distilled water for 1 day and then dried in vacuo and weighed (W_t). The gel yield (%) was calculated using the equation

$$\text{Degree of photocuring ratio (\%)} = W_t / W_0 \times 100$$

In vitro printing acellular constructs

The DNP printer was mainly consisted of a DMD chip (Discovery 4100, Texas instruments, USA) with a resolution of 1024 × 768 and a 980-nm NIR light source (Changchun Laser Optoelectronics Technology Co., China). The construct models were established and were then sliced into images using Creation Workshop software. These images were sent into the DMD chip using Discovery 4100 GUI software. After adding the bioink (15 wt % GelMA and 1 wt %

UCNP@LAP nanoinitiators) to the printing platform, the platform was moved and fastened to the designated position. A 200- μm -thick layer was printed by the exposure of patterned NIR light excited from DMD for 15 s. For fabrication of a multilayer structure, after the first layer was printed completely, the platform was moved down 200 μm . The same volume of the bioink was added and exposed by NIR light with the second-layer pattern. Repeating this procedure, multilayer construct can be fabricated.

To mimic the phenomena of the noninvasive in vivo 3D bioprinting, a piece of nude mice skin or 0.5-mm-thick pig muscle tissue was covered on the 40 μl of bioink, containing 15 wt % GelMA and 1 wt % UCNP@LAP nanoinitiators, and then printed into circle constructs. The exposure time for printing the circle constructs from the bioink covered by skin or pork muscle tissue is about 20 and 40 s, respectively. To quantify the extent of defect of the construct that printed from the bioink covered by muscle, ImageJ software was used for calculating the areas of the printed constructs. The A_{con} means the area of the circle construct that printed from bioink without any tissue cover. A_{m} means the area of the circle construct that printed from the bioink covered by muscle. The extent of the defect (ED_{m}) can be counted from the following equation: $(A_{\text{con}} - A_{\text{m}})/A_{\text{con}} \times 100\%$.

Cell culture

Articular chondrocytes (45) and ASCs (32) were isolated from newborn rat and 8-week-old BALB/c mice, respectively. The cells were cultured in a regular growth medium Dulbecco's modified Eagle's medium, a low-glucose medium supplemented with 10% fetal bovine serum at 37°C in a humidified and 5% CO₂ incubator. The cells were routinely harvested by treatment with an EDTA solution (0.25%).

Cell viability assay

Ear-shape constructs were printed with the bioink, containing 15 wt % GelMA, 1 wt % UCNP@LAP nanoinitiators, and $1 \times 10^6 \text{ ml}^{-1}$ cells chondrocytes. Cytocompatibility was tested with time as indicated by staining the cell-containing samples using a Live/Dead staining kit (Jiangsu KeyGEN BioTECH Corp.) according to the manufacturer's protocol. The tissue constructs were stained with 2 μM calcein (live-cell stain) and 8 μM propidium iodide (dead-cell stain) solution at room temperature for 30 min. After the incubation, the samples were washed with phosphate-buffered saline (PBS) thrice. Fluorescence images of the samples were recorded using a Leica DMI6000B microscope immediately.

In vivo bioprinting of acellular constructs

Eight-week-old BALB/c mice were narcotized, followed by removal of hair. Sterile N₂ gas was subcutaneously injected into the mice to isolate the skin and muscle tissue to create a cavity. Fifty microliters of the bioink (15 wt % GelMA and 1 wt % UCNP@LAP nanoinitiators in PBS) was subcutaneously injected into the cavity using a microsyringe. Then, the mice were fastened into the designated site of a printer under anesthesia. The injection site was irradiated by the patterned NIR light excited from the DMD chip controlled using a computer for 20 s. For the fabrication of a two-layer construct in vivo, first, 50 μl of the precursor solution was injected into the cavity and irradiated by patterned NIR light to print the first layer of the construct. Then, another 50 μl of precursor solution was injected into the irradiated site, and the second layer was printed. The

mice were sacrificed, and the images of the constructs stained with vitamin B12 were recorded using a camera.

Immunohistochemical staining for H&E

The collected tissues were fixed with a 4% paraformaldehyde (PFA) phosphate buffer solution overnight at room temperature. The samples were washed in running tap water, dehydrated in graded ethyl alcohol, and washed in xylene. The tissues were sealed in paraffin, cut into 4- μm -thick slices using a microtome, and stained with H&E. The samples were then imaged using a Leica DMI6000B microscope.

In vivo fabrication of ear-shaped living construct

Eight-week-old BALB/c nude mice were narcotized. Sterile N₂ gas was subcutaneously injected into the left back of mice to isolate the skin and muscle tissues to create a cavity. Fifty microliters of $1 \times 10^7 \text{ cells ml}^{-1}$ chondrocytes-containing bioink was injected into the cavity through a microsyringe. Then, the mice were fastened into the designated site of printer. The injected site was irradiated using the ear-shaped NIR light excited from the DMD chip for 20 s. Normal saline (NS) was injected into the back of mice near the irradiation site and sucked out to remove the uncured bioink. After 1 month, the samples were harvested and subjected to histological and immunohistochemical analyses. The tissue constructs were fixed with 4% PFA for 30 min and then dehydrated in 30% sucrose solution at 4°C overnight. The dehydrated samples were embedded in the optimal cutting temperature compound and frozen at -80°C overnight. The frozen samples were then cryo-sectioned. The sections were then stained with H&E for histological structure analyses. Type II collagen expression was detected using a rat anti-rabbit type II collagen polyclonal antibody (1:200; Invitrogen), followed by a horseradish peroxidase-conjugated anti-mouse antibody (1:50), and then colorized with diaminobenzidine tetrahydrochloride.

Excisional internal muscle wound healing model

Eight-week-old BALB/c mice were narcotized, followed by removal of hair. Surgeries were performed to open the skin at the dorsum of mice. An about 8-mm triangle muscle wound was excised using a scalpel and dissecting scissors followed by skin suture. Then, the outline of the wound was drawn in situ on the skin using a marker pen. After 24 hours, 100 μl of $1 \times 10^7 \text{ cells ml}^{-1}$ ASC-containing bioink was injected subcutaneously into the muscle wound. Then, the mice were fastened into the designated site of the printer under anesthesia. The injection site was irradiated by the patterned triangle NIR light excited from the DMD chip for 20 s. NS was injected into the back of mice near the irradiation site and sucked out to remove the uncured bioink. All the mice were euthanized after 10 days, digital photographs were taken, and the wound area was measured using ImageJ software. Wounds from the mice were used for histological analysis. To show whether this treatment could cause significant systemic toxicity in vivo, the major organs, including the heart, lung, liver, spleen, and kidney, were subjected to histopathological study by H&E staining.

Statistical analysis

Student's *t* test was carried out to examine the difference between two experimental groups such as treatment and control groups. All the data in this study are expressed as the mean values \pm SD. $P < 0.05$ was considered to be statistically significant.

SUPPLEMENTARY MATERIALS

Supplementary material for this article is available at <http://advances.sciencemag.org/cgi/content/full/6/23/eaba7406/DC1>

REFERENCES AND NOTES

1. L. Moroni, J. A. Burdick, C. Highley, S. J. Lee, Y. Morimoto, S. Takeuchi, J. J. Yoo, Biofabrication strategies for 3D in vitro models and regenerative medicine. *Nat. Rev. Mater.* **3**, 21–37 (2018).
2. X. Ma, J. Liu, W. Zhu, M. Tang, N. Lawrence, C. Yu, M. Gou, S. Chen, 3D bioprinting of functional tissue models for personalized drug screening and in vitro disease modeling. *Adv. Drug Deliv. Rev.* **132**, 235–251 (2018).
3. J. Koffler, W. Zhu, X. Qu, O. Platoshyn, J. N. Dulin, J. Brock, L. Graham, P. Lu, J. Sakamoto, M. Marsala, S. Chen, M. H. Tuszynski, Biomimetic 3D-printed scaffolds for spinal cord injury repair. *Nat. Med.* **25**, 263–269 (2019).
4. B. Derby, Printing and prototyping of tissues and scaffolds. *Science* **338**, 921–926 (2012).
5. A. Lee, A. R. Hudson, D. J. Shiwarski, J. W. Tashman, T. J. Hinton, S. Yerneni, J. M. Bliley, P. G. Campbell, A. W. Feinberg, 3D bioprinting of collagen to rebuild components of the human heart. *Science* **365**, 482–487 (2019).
6. M. Singh, H. M. Haverinen, P. Dhagat, G. E. Jabbour, Inkjet printing—process and its applications. *Adv. Mater.* **22**, 673–685 (2010).
7. R. D. Farahani, M. Dubé, D. Theriault, Three-dimensional printing of multifunctional nanocomposites: Manufacturing techniques and applications. *Adv. Mater.* **28**, 5794–5821 (2016).
8. Y. Zhang, F. Zhang, Z. Yan, Q. Ma, X. Li, Y. Huang, J. A. Rogers, Printing, folding and assembly methods for forming 3D mesostructures in advanced materials. *Nat. Rev. Mater.* **2**, 17019 (2017).
9. S. H. Kim, Y. K. Yeon, J. M. Lee, J. R. Chao, Y. J. Lee, Y. B. Seo, M. T. Sultan, O. J. Lee, J. S. Lee, S.-i. Yoon, I.-S. Hong, G. Khang, S. J. Lee, J. J. Yoo, C. H. Park, Precisely printable and biocompatible silk fibroin bioink for digital light processing 3D printing. *Nat. Commun.* **9**, 1620 (2018).
10. A. P. Zhang, X. Qu, P. Soman, K. C. Hribar, J. W. Lee, S. Chen, S. He, Rapid fabrication of complex 3D extracellular microenvironments by dynamic optical projection stereolithography. *Adv. Mater.* **24**, 4266–4270 (2012).
11. M. Gou, X. Qu, W. Zhu, M. Xiang, J. Yang, K. Zhang, Y. Wei, S. Chen, Bio-inspired detoxification using 3D-printed hydrogel nanocomposites. *Nat. Commun.* **5**, 3774 (2014).
12. Y. Yang, T. Du, J. Zhang, T. Kang, L. Luo, J. Tao, Z. Gou, S. Chen, Y. Du, J. He, S. Jiang, Q. Mao, M. Gou, A 3D-engineered conformal implant releases DNA nanocomplex for eradicating the postsurgery residual glioblastoma. *Adv. Sci.* **4**, 1600491 (2017).
13. V. V. Rocheva, A. V. Koroleva, A. G. Savelyev, K. V. Khaydukov, A. N. Generalova, A. V. Nechaev, A. E. Guller, V. A. Semchishen, B. N. Chichkov, E. V. Khaydukov, High-resolution 3D photopolymerization assisted by upconversion nanoparticles for rapid prototyping applications. *Sci. Rep.* **8**, 3663 (2018).
14. R. Polanía, M. A. Nitsche, C. C. Ruff, Studying and modifying brain function with non-invasive brain stimulation. *Nat. Neurosci.* **21**, 174–187 (2018).
15. Z. F. Gao, E. E. Sann, X. Lou, R. Liu, J. Dai, X. Zuo, F. Xia, L. Jiang, Naked-eye point-of-care testing platform based on a pH-responsive superwetting surface: Toward the non-invasive detection of glucose. *NPG Asia Mater.* **10**, 177–189 (2018).
16. J. Tao, J. Zhang, T. Du, X. Xu, X. Deng, S. Chen, J. Liu, Y. Chen, X. Liu, M. Xiong, Y. Luo, H. Cheng, J. Mao, L. Cardon, M. Gou, Y. Wei, Rapid 3D printing of functional nanoparticle-enhanced conduits for effective nerve repair. *Acta Biomater.* **90**, 49–59 (2019).
17. L. G. Bracaglia, M. Messina, S. Winston, C.-Y. Kuo, M. Lerman, J. P. Fisher, 3D printed pericardium hydrogels to promote wound healing in vascular applications. *Biomacromolecules* **18**, 3802–3811 (2017).
18. G. Chen, H. Qiu, P. N. Prasad, X. Chen, Upconversion nanoparticles: Design, nanotechnology, and applications in theranostics. *Chem. Rev.* **114**, 5161–5214 (2014).
19. S. Xu, X. Zhu, C. Zhang, W. Huang, Y. Zhou, D. Yan, Oxygen and Pt(II) self-generating conjugate for synergistic photo-chemo therapy of hypoxic tumor. *Nat. Commun.* **9**, 2053 (2018).
20. N. W. S. Kam, M. Connell, J. A. Wisdom, H. Dai, Carbon nanotubes as multifunctional biological transporters and near-infrared agents for selective cancer cell destruction. *Proc. Natl. Acad. Sci. U.S.A.* **102**, 11600–11605 (2005).
21. A. L. Antaris, H. Chen, K. Cheng, Y. Sun, G. Hong, C. Qu, S. Diao, Z. Deng, X. Hu, B. Zhang, X. Zhang, O. K. Yaghi, Z. R. Alamparambil, X. Hong, Z. Cheng, H. Dai, A small-molecule dye for NIR-II imaging. *Nat. Mater.* **15**, 235 (2015).
22. F. Wang, Y. Han, C. S. Lim, Y. Lu, J. Wang, J. Xu, H. Chen, C. Zhang, M. Hong, X. Liu, Simultaneous phase and size control of upconversion nanocrystals through lanthanide doping. *Nature* **463**, 1061–1065 (2010).
23. S. Chen, A. Z. Weitemier, X. Zeng, L. He, X. Wang, Y. Tao, A. J. Y. Huang, Y. Hashimoto, M. Kano, H. Iwasaki, L. K. Parajuli, S. Okabe, D. B. L. Teh, A. H. Ali, I. Tsutsui-Kimura, K. F. Tanaka, X. Liu, T. J. McHugh, Near-infrared deep brain stimulation via upconversion nanoparticle-mediated optogenetics. *Science* **359**, 679–684 (2018).
24. L. M. Jin, X. Chen, C. K. Siu, F. Wang, S. F. Yu, Enhancing multiphoton upconversion from NaYF₄:Yb/Tm@NaYF₄ core-shell nanoparticles via the use of laser cavity. *ACS Nano* **11**, 843–849 (2017).
25. B. D. Fairbanks, M. P. Schwartz, C. N. Bowman, K. S. Anseth, Photoinitiated polymerization of PEG-diacrylate with lithium phenyl-2,4,6-trimethylbenzoylphosphine: Polymerization rate and cytocompatibility. *Biomaterials* **30**, 6702–6707 (2009).
26. J.-W. Kim, E.-H. Kim, G.-D. Han, S.-H. Noh, D.-G. Pyun, Y. Ito, J.-W. Nah, J.-G. Lee, T.-I. Son, Preparation of UV-curable alginate derivatives for drug immobilization on dressing foam. *J. Ind. Eng. Chem.* **54**, 350–358 (2017).
27. J. R. Tumbleston, D. Shirvanyants, N. Ermoshkin, R. Januszewicz, A. R. Johnson, D. Kelly, K. Chen, R. Pinschmidt, J. P. Rolland, A. Ermoshkin, E. T. Samulski, J. M. DeSimone, Continuous liquid interface production of 3D objects. *Science* **347**, 1349–1352 (2015).
28. A. A. Pawar, S. Halivni, N. Waiskopf, Y. Ben-Shahar, M. Soreni-Harari, S. Bergbreiter, U. Banin, S. Magdassi, Rapid three-dimensional printing in water using semiconductor-metal hybrid nanoparticles as photoinitiators. *Nano Lett.* **17**, 4497–4501 (2017).
29. G. Zhou, H. Jiang, Z. Yin, Y. Liu, Q. Zhang, C. Zhang, B. Pan, J. Zhou, X. Zhou, H. Sun, D. Li, A. He, Z. Zhang, W. Zhang, W. Liu, Y. Cao, In vitro regeneration of patient-specific ear-shaped cartilage and its first clinical application for auricular reconstruction. *EBioMedicine* **28**, 287–302 (2018).
30. H.-W. Kang, S. J. Lee, I. K. Ko, C. Kengla, J. J. Yoo, A. Atala, A 3D bioprinting system to produce human-scale tissue constructs with structural integrity. *Nat. Biotechnol.* **34**, 312–319 (2016).
31. M. Y. Park, J. S. Choi, K. S. Kim, S. Rhim, H. J. Park, M. K. Shin, Identification of a closed cutaneous injury after mechanical trauma caused by collision. *Skin Res. Technol.* **25**, 440–446 (2019).
32. S. A. Castleberry, B. D. Almquist, W. Li, T. Reis, J. Chow, S. Mayner, P. T. Hammond, Self-assembled wound dressings silence MMP-9 and improve diabetic wound healing in vivo. *Adv. Mater.* **28**, 1809–1817 (2016).
33. W. M. Jackson, L. J. Nesti, R. S. Tuan, Concise review: Clinical translation of wound healing therapies based on mesenchymal stem cells. *Stem Cells Transl. Med.* **1**, 44–50 (2012).
34. B. E. Kelly, I. Bhattacharya, H. Heidari, M. Shusteff, C. M. Spadaccini, H. K. Taylor, Volumetric additive manufacturing via tomographic reconstruction. *Science* **363**, 1075–1079 (2019).
35. S. K. Saha, D. Wang, V. H. Nguyen, Y. Chang, J. S. Oakdale, S.-C. Chen, Scalable submicrometer additive manufacturing. *Science* **366**, 105–109 (2019).
36. B. Grigoryan, S. J. Paulsen, D. C. Corbett, D. W. Sazer, C. L. Fortin, A. J. Zaita, P. T. Greenfield, N. J. Calafat, J. P. Gounley, A. H. Ta, F. Johansson, A. Randles, J. E. Rosenkrantz, J. D. Louis-Rosenberg, P. A. Galie, K. R. Stevens, J. S. Miller, Multivascular networks and functional intravascular topologies within biocompatible hydrogels. *Science* **364**, 458–464 (2019).
37. S. Shanmugam, J. Xu, C. Boyer, Light-regulated polymerization under near-infrared/far-red irradiation catalyzed by bacteriochlorophyll a. *Angew. Chem. Int. Ed.* **55**, 1036–1040 (2016).
38. A. H. Bonardi, F. Dumur, T. M. Grant, G. Noirbent, D. Gimes, B. H. Lessard, J. P. Fouassier, J. Lalevée, High performance near-infrared (NIR) photoinitiating systems operating under low light intensity and in the presence of oxygen. *Macromolecules* **51**, 1314–1324 (2018).
39. S. Beyazit, S. Ambrosini, N. Marchyk, E. Palo, V. Kale, T. Soukka, B. Tse Sum Bui, K. Haupt, Versatile synthetic strategy for coating upconverting nanoparticles with polymer shells through localized photopolymerization by using the particles as internal light sources. *Angew. Chem. Int. Ed.* **53**, 8919–8923 (2014).
40. F. Wang, J. Wang, X. Liu, Direct evidence of a surface quenching effect on size-dependent luminescence of upconversion nanoparticles. *Angew. Chem. Int. Ed.* **122**, 7618–7622 (2010).
41. X. Liu, J. Tao, J. Liu, X. Xu, J. Zhang, Y. Huang, Y. Chen, J. Zhang, D. Y. B. Deng, M. Gou, Y. Wei, 3D printing enabled customization of functional microgels. *ACS Appl. Mater. Interfaces* **11**, 12209–12215 (2019).
42. J. Tao, X. Xu, S. Wang, T. Kang, C. Guo, X. Liu, H. Cheng, Y. Liu, X. Jiang, J. Mao, M. Gou, Polydiacetylene-nanoparticle-functionalized microgels for topical bacterial infection treatment. *ACS Macro Lett.* **8**, 563–568 (2019).
43. M. Montgomery, S. Ahadian, L. Davenport Huyer, M. Lo Rito, R. A. Civitarese, R. D. Vanderlaan, J. Wu, L. A. Reis, A. Momen, S. Akbari, A. Pahnke, R.-K. Li, C. A. Caldarone, M. Radisic, Flexible shape-memory scaffold for minimally invasive delivery of functional tissues. *Nat. Mater.* **16**, 1038–1046 (2017).
44. H. Shirahama, B. H. Lee, L. P. Tan, N.-J. Cho, Precise tuning of facile one-pot gelatin methacryloyl (GelMA) synthesis. *Sci. Rep.* **6**, 31036 (2016).

45. Y. Liu, L. Zhang, G. Zhou, Q. Li, W. Liu, Z. Yu, X. Luo, T. Jiang, W. Zhang, Y. Cao, In vitro engineering of human ear-shaped cartilage assisted with CAD/CAM technology. *Biomaterials* **31**, 2176–2183 (2010).

Acknowledgments: We thank H. Wang from the Analytical and Testing Center, Sichuan University, P. R. China for the SEM observation and analysis of the data. **Funding:** This work was supported by Key Research and Development Projects of People's Liberation Army (BWS17J036), the Science and Technology Project of Chengdu (2018-CY02-00041-GX), the National Natural Science Foundation (31525009), National Key R&D Program of China (2017YFA0104800) 1-3-5 project for disciplines of excellence, and West China Hospital, Sichuan University (ZYJC18017, ZYYC08007). **Author contributions:** M.G., Z.Q., and X.W. designed and supervised the project. S.C., X.X., X.Li, L.C., and S.W. contributed to design experiments and discuss results. Y.C., J.Z., X.Liu, J.T., Y.H., W.W., Y.L., and K.Z. performed experiments. M.G., Y.C., J.Z., X.Liu, S.W., X.W., and S.C. wrote the manuscript. **Competing interests:** M.G., Y.C., and

J.Z. are inventors on two patents under preliminary review related to this work, filed by the National Intellectual Property Administration, PRC (no. 201710558327.4 2, 10 July 2017 and no. 201711378409.7, 19 December 2017). All other authors declare that they have no competing interests. **Data and materials availability:** All data needed to evaluate the conclusions in the paper are present in the paper and/or the Supplementary Materials. Additional data related to this paper may be requested from the authors.

Submitted 31 December 2019

Accepted 6 April 2020

Published 5 June 2020

10.1126/sciadv.aba7406

Citation: Y. Chen, J. Zhang, X. Liu, S. Wang, J. Tao, Y. Huang, W. Wu, Y. Li, K. Zhou, X. Wei, S. Chen, X. Li, X. Xu, L. Cardon, Z. Qian, M. Gou, Noninvasive in vivo 3D bioprinting. *Sci. Adv.* **6**, eaba7406 (2020).

Noninvasive in vivo 3D bioprinting

Yuwen Chen, Jiumeng Zhang, Xuan Liu, Shuai Wang, Jie Tao, Yulan Huang, Wenbi Wu, Yang Li, Kai Zhou, Xiawei Wei, Shaochen Chen, Xiang Li, Xuewen Xu, Ludwig Cardon, Zhiyong Qian and Maling Gou

Sci Adv 6 (23), eaba7406.
DOI: 10.1126/sciadv.aba7406

ARTICLE TOOLS

<http://advances.sciencemag.org/content/6/23/eaba7406>

SUPPLEMENTARY MATERIALS

<http://advances.sciencemag.org/content/suppl/2020/06/01/6.23.eaba7406.DC1>

REFERENCES

This article cites 45 articles, 8 of which you can access for free
<http://advances.sciencemag.org/content/6/23/eaba7406#BIBL>

PERMISSIONS

<http://www.sciencemag.org/help/reprints-and-permissions>

Use of this article is subject to the [Terms of Service](#)

Science Advances (ISSN 2375-2548) is published by the American Association for the Advancement of Science, 1200 New York Avenue NW, Washington, DC 20005. The title *Science Advances* is a registered trademark of AAAS.

Copyright © 2020 The Authors, some rights reserved; exclusive licensee American Association for the Advancement of Science. No claim to original U.S. Government Works. Distributed under a Creative Commons Attribution NonCommercial License 4.0 (CC BY-NC).